Metal fluorides passivate II-VI and III-V quantum dots

Rodolphe Valleix, [†,‡] William Zhang, [†] Lilian Guillemeney, [‡] Abraham J. Jordan, [†] Leslie G. Castro, [†] Bereket L. Zekarias, [†] Sungho V. Park, [†] Oliver Wang, [†] and Jonathan S. Owen [†] *

[†] Department of Chemistry, Columbia University, New York, NY 10027, United States.

[‡] Univ. Lyon, ENS de Lyon, CNRS, Laboratoire de Chimie, F-69342, Lyon, France.

ABSTRACT: The interaction between II-VI and III-V quantum dots (QDs) and metal fluorides is investigated using optical absorption, photoluminescence, and nuclear magnetic resonance spectroscopies. QDs with metal fluoride passivated surfaces were prepared by ligand exchange with anhydrous oleylammonium fluoride. The photoluminescence quantum yield (PLQY) of II-VI QD cores and core-shell structures are dramatically enhanced following ligand exchange, near unity in some cases, but only after exposure to air. In the case of InP QDs, oleylammonium fluoride induces a gradual etching of the crystal, yielding oleylamine, PH_3, and InF_3 coproducts, resulting in a remarkable increase in PLQY (up to 83%). The frequency and breadth of $\nu(N–H)$ bands in the infrared spectrum supports the assignment of oleylamine ligand binding to InP. The fluoride content (1.6–9.2 nm^{-2}) is compared with the coverage of oleylamine ligands (2.3–5.1 nm^{-2}) and demonstrates the formation of surfaces densely covered by metal fluoride and amine ligands. The relationship between the electrophilicity and small steric profile of metal fluoride surface ligands and their surface passivating effects on QDs is discussed.

1

2

II-VI and III-V Quantum Dots (QDs) are cutting edge color converters in luminescent displays and warm spectrum solid-state lighting devices. [1, 2] Their exceptional performance is characterized by a narrow spectral linewidth, high brightness, and stability. Each of these performance characteristics, and especially the photoluminescence quantum yield (PLQY), are influenced by the crystal's surface and its interaction with surface ligands.[3, 4] This has led to exploration of ligands and surface structures that can increase the performance of luminescent QDs.

Metal halide and/or metal carboxylate complexes are recognized among surface ligands for their ability to enhance the PLQY. This improvement can be attributed to the reduction of mid-band gap states induced by exposed chalcogenide surface atoms, which cause hole trapping.[5-8] Halides in particular, are compact ligands that are better suited to the high aerial density of atoms on binary semiconductor surfaces. By comparison, the steric bulk of organic ligands can prevent them from achieving high surface coverages and result in relatively week binding affinity.[9] For instance, the adsorption of metal chlorides onto CdTe nanocrystals can result in near unity quantum yields, while alkylammonium halide adsorption is less effective.[8]

The electrophilicity of halide ligands is known to reduce the band edge potentials of semiconductor nanocrystals,[10] which can help stabilize QDs against aerobic decomposition in air.[11, 12] While nanocrystals with chloride, bromide, and iodide ligands are common, there is comparatively less information about the binding and passivation of surfaces with fluoride ligands, despite their greater electronegativity.[13] Fluorides are also more compact than the other halides, which could allow higher aerial packing densities and stronger binding affinities than other metal halides or carboxylate passivating layers. A high packing density can help ensure better surface passivation and afford greater chemical inertness. Metal fluoride passivated QDs, are therefore,

3

interesting candidates for solid-state lighting and display devices where degradation in air remains a significant limitation to their performance.[14, 15]

Fluoride terminated nanocrystal surfaces have been prepared via ligand exchange with a variety of fluoride sources. For example, photochemical or thermal etching of InP nanocrystals with aqueous hydrofluoric acid (HF)[16, 17] has been used to remove surface oxide impurities and increase the PLQY.[18-20] Safer alternatives to aqueous hydrogen fluoride have been pursued, including ionic liquids, [21, 22] ammonium fluoride/bifluoride, [23] zinc fluoride and carboxylic acids, [24] hexafluorophosphate ions, [25] and benzoyl fluoride. [26] These approaches also increase the PLQY of the InP core nanocrystals up to as much as 70%. [26] However, it is unclear whether the PLQY enhancement is caused by removal of surface oxides or the binding of metal fluoride ligands to the QD surface. Notably, it has been reported that adding $ZnCl_2$ to InP QDs in the presence of fluoride further increases the PLQY to 80%. In addition, InP/ZnSe/ZnS QDs grown in the presence of ZnF_2 and ZnTe/ZnSe/ZnS QDs grown in the presence of $HF/ZnCl_2$ achieve PLQYs > 90% and record electroluminescence quantum efficiencies.[24, 27] Together these observations suggested that metal fluoride binding to the zinc chalcogenides may passivate the QD surface. We therefore sought to understand the role of fluoride in the passivation of both III-V and II-VI QDs.

In the present study we investigated the reaction of InP and II-VI QDs with anhydrous oleylammonium fluoride ([Oleyl-NH_3]$^+$[F]$^-$) prepared from benzoyl fluoride and oleylamine according to Scheme 1. A stoichiometry of 2 amines per benzoyl fluoride produces oleylbenzamide and [R-NH_3]$^+$[F]$^-$ *in situ* as can be observed using ^{1}H and ^{19}F NMR spectroscopies (Figure S1). The reaction of [Oleyl-NH_3]$^+$[F]$^-$ and InP caused slow etching of the crystal that is accelerated by heating the mixture or irradiation (λ_{max} = 427 nm). A steady blue shift in the band

4

edge photoluminescence is accompanied by a narrowing and increase in the PLQY, and a steady

reduction of the absorbance at higher energy ($\lambda = 413$ nm) over several hours (Figures 1 and S2).
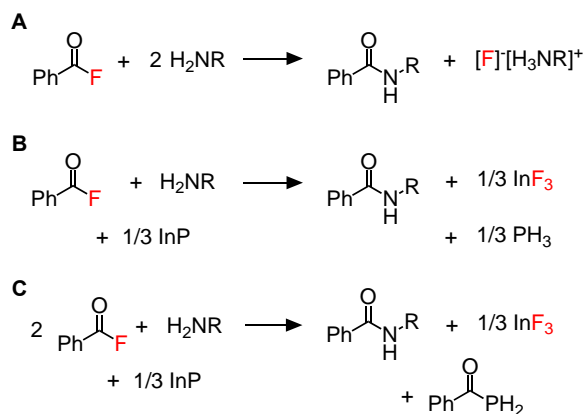
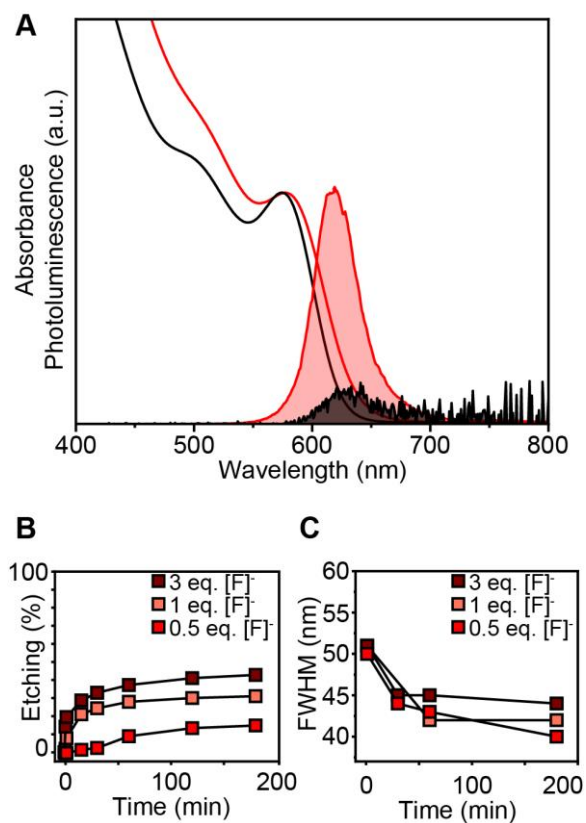**Scheme 1.** Stoichiometry of reactions between benzoyl fluoride, oleylamine and InP.

Figure 1. (A) UV-Vis and PL spectra of InP QDs before (black) and after (red) etching with [Oleyl-NH$_3$]$^+$[F]$^-$. (B) Extent of etching with time QDs as measured by UV-Vis ($\lambda = 413$ nm). (C) Evolution of the photoluminescence FWHM over time.

The narrowing of the photoluminescence and the increase in the PLQY observed for III-V QDs led us to attempt similar reactions with II-VI QDs and core-shell heterostructures (Table 1). CdS, CdSe, ZnSe, and core/shell QDs were synthesized from metal oleate and chalcogenourea precursors[28, 29] and combined with [Oleyl-NH$_3$]$^+$[F]$^-$. In all cases, the PLQY increases and the broad trap emission is eliminated, without significantly changing the total absorption or shifting the luminescence wavelength (Figures S3 and S4). Similar results were obtained at room temperature and in the dark indicating that changes to the PLQY result from surface ligand exchange rather than etching.

Table 1. Optical properties of QDs following reaction with [Oleyl-NH$_3$]$^+$[F]$^-$.

QD	PL-λ_{max} (nm)	$fwhm$ (nm)	Before PLQY (%)	After PLQY (%)
InP	625	41 $\leq$	<2	≤ 83
CdS	485	16	5	$\leq 62^a$
CdSe	631	30	26	35
ZnSe	374	17	<1	14
CdS/CdSe/CdS	547	38	62	82
CdS/CdSe/CdS	624	32	88	97
InP/ZnS	624	55	33	82

^{a} See Figure S5 for complete list of conditions and PLQY values.

6

The kinetics of etching InP were monitored using absorption and photoluminescence spectroscopies (Figure 1). The rate and extent of etching increases with the amount of added [Oleyl-NH$_3$]$^+$[F]$^-$ and reaches completion in two–three hours. The kinetics are more rapid if substoichiometric amine (Scheme 1B and 1C) is used, however, substantial spectral broadening and an increase in the size distribution is observed (ESI section S3 and Figures S6 & S24 - 27). The linewidth can be preserved if stoichiometric amine is used to cleave benzoyl fluoride (2 equiv. / fluoride, Scheme 1A) and fewer equivs. of [Oleyl-NH$_3$]$^+$[F]$^-$ are used. For example, 1 equivalent of [Oleyl-NH$_3$]$^+$[F]$^-$ per InP unit causes a reduction of the FWHM from > 50 to 42 nm and an increase in the PLQY to 53 %. Even lower amounts of [Oleyl-NH$_3$]$^+$[F]$^-$ did not improve the PLQY nor the FWHM, however fluoride can be consumed by reaction with surfactants, excess metal salts, and glassware so the behavior at low equivalents depend on the conditions of the experiment. Under slow and controlled etching conditions, the tetrahedral shape, size, crystal structure and polydispersity of the QDs are maintained (Figures S7 and S8).

The changes in the photoluminescence linewidth can be attributed to elimination of broad trap luminescence which represents a significant fraction of the luminescence of InP QDs with low PLQY. We also probed the size dependence of the etching reactivity to determine whether etching was accompanied by size distribution focusing. The kinetics of etching for several different sizes and different capping ligands were studied, providing evidence that small InP QDs ($\lambda_{1s\text{-}1s}$ = 540 nm) undergo more rapid etching (moles [InP]$_i$/sec) than large InP QDs ($\lambda_{1s\text{-}1s}$ = 583 nm) under otherwise identical conditions (Figure S28 and S30). More rapid reaction of smaller QDs can increase the polydispersity, contrary to the narrowing of the FWHM observed herein. Hence, the narrowing observed in figure 1C results from a decrease of trap luminescence to the overall spectral linewidth rather than a result of size distribution focusing. Nonetheless, lower

7

concentrations of fluoride and stoichiometric amine improve the selectivity of the etching process and preserve the polydispersity.

The PLQY increases with the extent of etching, reaching as high as 83% at 3 eq. of added benzoyl fluoride per unit of InP, the highest reported PLQY for an InP QD without a shell. {Yadav, 2023 #53} Although the increased PLQY could be explained by the removal of impurities (*e.g.* oxidized phosphorus), this explanation does not explain why the PLQY steadily increases as the QD shrinks. Alternatively, InF_3 produced by the etching reaction may bind and passivate the QD surface. A steadily increasing concentration of metal fluoride ligands produced by etching could increase their coverage during the etching reaction. To test this hypothesis we investigated the adsorption of metal fluoride complexes to the surface of CdS QDs where the reaction with [Oleyl-NH$_3$]$^+$[F]$^-$ does not etch the QD core.

The reaction of CdS nanocrystals with [Oleyl-NH$_3$]$^+$[F]$^-$ displaces oleate ligands without changing the optical absorption spectrum. The vinyl region of the ^{1}H NMR spectrum of the ligand exchange mixture (Figure S9) shows that roughly half of the oleate ligands are freely diffusing in solution upon addition of [*n*-octyl-NH$_3$]$^+$[F]$^-$ (1 equiv. [F]$^-$/(CdS)$_i$) (Figure S9). Despite this drop in the oleate coverage the PLQY increases. In comparison, using tetramethylethylene diamine to displace cadmium oleate ligands from CdS-Cd(O$_2$CR)$_2$ causes a precipitous drop in the PLQY.[5] The difference in PLQY suggests that [R-NH$_3$]$^+$[F]$^-$ (R = oleyl, *n*-octyl) displaces oleic acid, rather than cadmium oleate, and forms surface bound cadmium fluoride that is responsible for the PLQY enhancement (Scheme 2). While no signals from surface bound fluoride were evident in the liquids ^{19}F NMR spectrum (see NMR discussion below), the XPS spectrum contains a signal at 684.9 eV which is consistent with the presence of CdF$_2$ (Figure S10).[30]

8
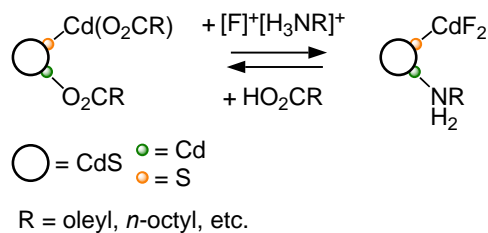
Scheme 2. Reaction of **CdS-Cd(O₂CR)₂** with [Oleyl-NH₃]⁺[F]⁻.

To avoid contamination by oxides the above experiments were performed under rigorous anaerobic conditions beginning from anhydrous cadmium oleate. Interestingly, under these conditions the PLQY was largely insensitive to the addition of [Oleyl-NH₃]⁺[F]⁻. However, if the solutions of CdS QDs and fluoride were exposed to air, the PLQY increased to as high as 62%. We further probed the influence of fluoride concentration on the PLQY and found that high fluoride concentrations caused a drop in PLQY unless additional cadmium oleate was added (Figure S5). This protective effect suggests that cadmium fluoride formed by the ligand exchange can bind the QD surface and enhance the PLQY.

We further explored the role of fluoride on the PLQY of InP QDs by carefully protecting InP nanocrystals from oxidation prior to reaction with [Oleyl-NH₃]⁺[F]⁻. Oxide free InP nanocrystals were prepared from *tris*(diethylamino)phosphine and indium and zinc halides in oleylamine, rather than indium carboxylate precursors that are known to form surface oxides.[31] However, oxides have also been detected in syntheses beginning from indium chloride and *tris*(diethylamino)phosphine, that can be attributed to air exposure and the use of ethanol during the purification and isolation procedure (Supporting Information).[32-35] To avoid oxidation and alcoholysis of the QD synthesis

9

mixture, a QD synthesis, purification, and isolation procedure was developed that rigorously protects the QDs from air and uses aprotic solvents.

Tetrahedral InP QDs prepared in this way are associated with *tetrakis*(oleylamino)phosphonium ions ($[P(NHR)_4]^+$, R = Oleyl) rather than amine ligands, and show little to no ^{31}P nuclear magnetic resonance (NMR) signals commonly attributed to oxides (Figure 2).[31] The ^1H and ^{31}P NMR signatures of $[P(NHR)_4]^+$ ($\delta = 29.5$ ppm, FWHM = 66 Hz) are similar to an independently prepared sample of *tetrakis*(*n*-hexylamino)phosphonium chloride ($\delta = 29.7$ ppm, FWHM = 52 Hz). Moreover, the ^1H NMR chemical shift of the resonance corresponding to the methylene alpha to nitrogen matches the ^1H NMR spectrum of *tetrakis*(*n*-hexylamino)phosphonium chloride ($\delta = 2.90$ ppm), rather than oleylamine ($\delta = 2.51$ ppm) or oleylammonium ions ($\delta = 3.09$ ppm) (Figure S11). We confirmed this assignment by adding authentic samples of oleylamine and oleylammonium chloride to the NMR tube of the purified QDs, which produced distinct ^1H NMR resonances (Figure S12). We conclude that QDs isolated from toluene and methyl acetate have a distinct surface termination than other samples of InP that are ligated by amines.[36, 37]
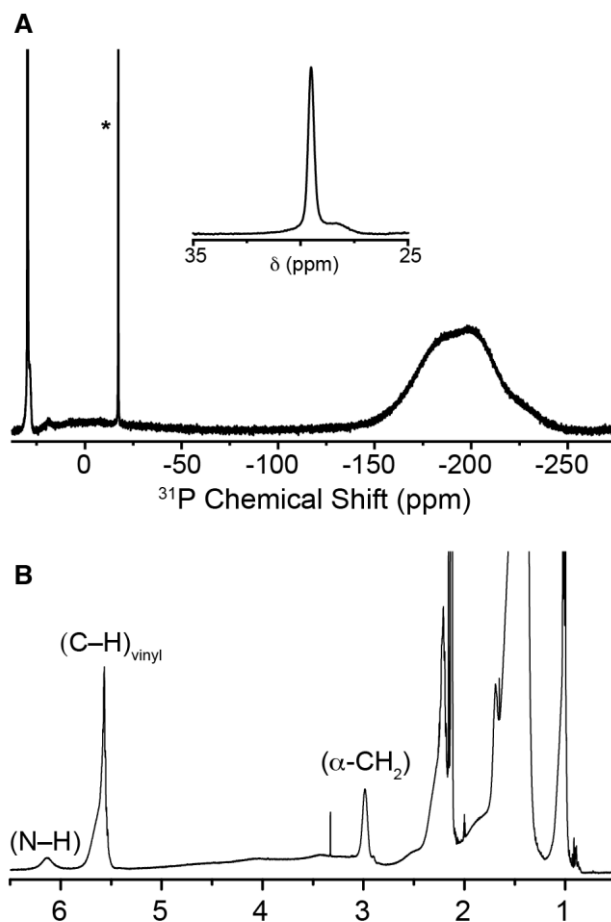
10

Figure 2. Solution-phase (a) ^{31}P and (b) ^{1}H NMR spectra of InP QDs purified 9x using toluene/methyl acetate. Internal standard resonances are present in ^{31}P NMR: δ(ppm): -17.43.

During purification the quantity of [P(NHR)$_4$]$^+$ ions decreases gradually to 0.4 nm^{-2} (2.2 oleyl chains nm^{-2}) as measured by integrating either the ^{1}H or ^{31}P NMR spectra relative to an internal standard (see Supporting Information). At the lower coverage the ^{31}P and ^{1}H NMR resonances of [P(NHR)$_4$]$^+$ ions split into two features, one broader than the other, suggesting two populations are present (Figure 2). Although in principle tightly and loosely bound counterions could explain the lineshape, the presence of metal halide complexes (*e.g.* [(ZnCl$_{2+x}$)$_m$]$^{mx-}$[P(NHR)$_4$]$_m^+$) may also

11

influence the spectrum. Difficulty separating the QDs from such an impurity may explain why most purification methods use ethanol, which efficiently removes an oily byproduct that is otherwise difficult to remove using aprotic solvents.

^{1}H and ^{31}P NMR diffusion ordered spectroscopy (DOSY) measurements of purified QDs (0.4 [P(NHR)$_4$]$^+$ nm^{-2}) provided a single diffusivity (230 μm²/s from ^{1}H DOSY) that is an order of magnitude slower than a triphenylphosphate internal standard, and 3 times faster than previous measurements on InP QDs.[36] A higher diffusivity might be expected from the component displaying a narrower NMR signal, while the broader component could have much slower diffusivity. Regardless, we conclude that [P(NHR)$_4$]$^+$ is associated with QDs reported here.

^{1}H and ^{31}P NMR spectroscopy was used to monitor the etching of InP *in situ*. The results of the etching depend on the amine stoichiometry as depicted in Scheme 1. For example, if only equivalent of amine is used, a benzoylphosphine coproduct is also detected that arises from a side reaction between PH$_3$ and benzoyl fluoride (Scheme 1 and Figure S13-S16).[38-40] ^{31}P NMR spectra obtained without ^{1}H decoupling confirm the presence of two attached hydrogens with a chemical shift and coupling constant that match literature values ([31]P δ = -109.6 ppm; [1]H δ = 3.9 ppm, $^1J_{P\text{-}H}$ = 218 Hz)).[41-43] In addition, when InP-InCl$_3$/P(NH-oleyl)$_4$Cl are treated with 1 equiv. of [Oleyl-NH$_3$]$^+$[F]$^-$ (Figure 3), two side products are observed that are assigned to a *bis*-(oleylamino)-*P,P*-difluorophosphonium cation ([F$_2$P(NHR)$_2$]$^+$) (^{19}F {^{1}H} NMR: δ = -63 ppm, $^1J_{F\text{-}P}$ = 640 Hz); ^{31}P {^{1}H} NMR: δ = -67 ppm; $^1J_{F\text{-}P}$ = 640 Hz) and a *bis*-phosphazene base ([(RNH)$_3$P-(NR)-P=NR(NHR)$_2$]$^+$, ^{31}P {^{1}H} NMR: δ = 16 ppm) on the basis of their ^{31}P and ^{19}F chemical shifts[44], $^1J_{F\text{-}P}$ coupling constants, and an electrospray ionization mass spectrum (ESI-MS). [F$_2$P(NHR)$_2$]$^+$ was independently synthesized from [P(NHR)$_4$]$^+$[Cl]$^-$ (R = *n*-hexyl) and [Oleyl-NH$_3$]$^+$[F]$^-$ and characterized with ^{19}F {^{1}H} and ^{31}P {^{1}H} NMR spectroscopy and ESI-MS (Figure S17). A similar

12

bis-phosphazene base may explain an NMR signal recently reported in a study of InP from a substoichiometric mixture of dimethylaminophosphine, indium chloride, and oleylamine.[45]
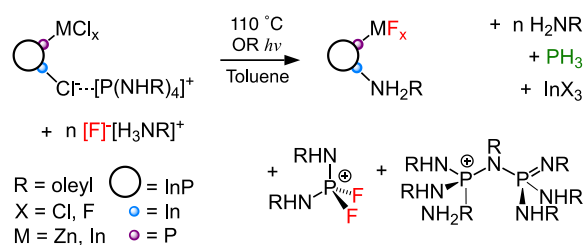
Scheme 3. Reaction between $[OleylNH_3]^+[F]^-$ and **InP-InCl$_3$/P(NH-oleyl)$_4$Cl**.
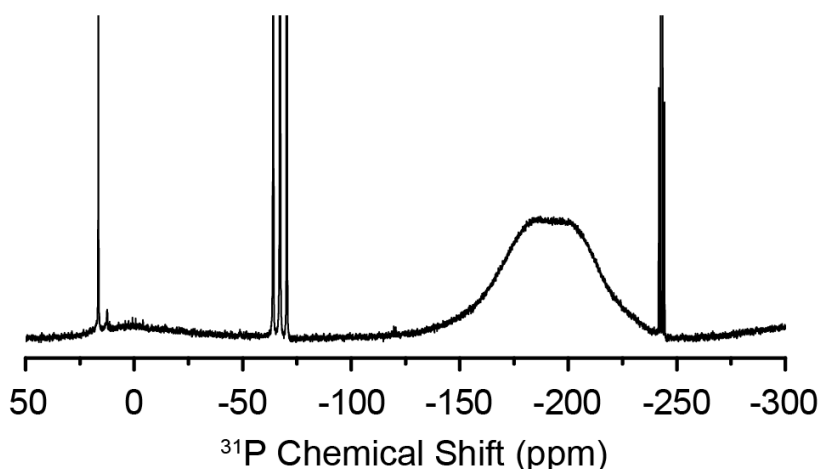
Figure 3. ^{31}P NMR spectrum of **InP-InCl$_3$/P(NH-oleyl)$_4$Cl** QDs during *in situ* etching using 1 equiv of $[Oleyl-NH_3]^+[F]^-$ in d_6-benzene. δ = -67 ppm ($[F_2P(NHR)_2]^+$); δ = 16 ppm ($[(RNH)_3P$-$(NR)-P=NR(NHR)_2]^+$); δ = -200.6 ppm (InP core) and δ = - 242.3 ppm (PH_3).

Thus, the InP lattice and $[P(NHR)_4]^+$ surfactants undergo acidolysis in the presence of $[Oleyl-NH_3]^+[F]^-$ producing an equivalent of PH_3 and InF_3 in the case of the nanocrystals. This conclusion is in line with previously published work,[26, 46] but distinct from proposals that etching proceeds by reaction of fluoride and lattice phosphorus atoms.[47, 48]

13

Metal fluorides (M = Zn, Cd, In) produced by the reaction with $[Oleyl-NH_3]^+[F]^-$ can bind the QD surface. X-ray photoelectron spectroscopy analysis of the product QDs supports the presence of the metal fluoride (Figures S10 and S18) coproducts (*e.g.* InF_3 (685.4 eV) and CdF_2 (684.9 eV)), but the liquids ^{19}F NMR spectra of these samples gave little to no fluorine signal. This is typical of extended inorganic fluorides whose ^{19}F NMR linewidth is broadened by chemical shift anisotropy and dipolar couplings.[49] In support of this conclusion, signals from inorganic fluoride are observed in magic angle spinning solid state NMR spectra that are enhanced using ^{31}P-^{19}F cross polarization, a finding that will be reported elsewhere. The lack of ^{19}F NMR signals without magic angle spinning is consistent with a metal fluoride bound to the QD surface.

To determine the amount of fluoride present, metal fluoride coated QDs were reacted with chlorotrimethylsilane ($Me_3Si–Cl$), which rapidly produces fluorotrimethylsilane ($Me_3Si–F$) owing to the strong Si–F bond (BDE(Si–F) = 160 kcal/mol *vs.* BDE(Si–Cl) = 117 kcal/mol[50], (^{19}F δ = -156.26 ppm; ^1H δ = 0.03 ppm; $J_{1H–19F}$ = 7.4 Hz) (Equation 1 and Figures S19 and S20). Additional $Me_3Si–Cl$ does not increase the yield of $Me_3Si–F$, indicating that all reactive fluoride is consumed in under an hour. The yield of $Me_3Si–F$ provides a lower bound on the amount of inorganic fluoride in the product QDs that can be expressed as a surface coverage (Table 2).

$$(InP)_n/MF_x + Cl–SiMe_3 \longrightarrow (InP)_n/MCl_x + F–SiMe_3 \tag{1}$$

Table 2. Fluoride and oleyl content InP QDs following fluorination and purification by precipitation.

$[R-NH_3]^+[F]^-$ (equiv.)	F (nm^{-2})	Oleyl (nm^{-2})	F : Oleyl	L (nm)
0.5	1.6 ± 0.1	2.3 ± 0.1	0.6	5.5
1	4.2	3.4	1.2	5.4

14

|			
	± 0.5	± 0.3		
3	9.2 ± 0.6	5.1 ± 0.9	1.8	5.4

a Densities are measured vs. an internal standard in d_8-toluene, using ^{1}H and ^{19}F NMR spectroscopy.

The fluoride coverage increases with the amount of [Oleyl-NH$_3$]$^+$[F]$^-$ used in the photochemical etching process and can exceed the aerial density of atoms on the <111> surface (6.3 nm^{-2}) and the packing density of crystalline *n*-aliphatic chains (4.9 nm^{-2}). Although precise determination of the chemical formulas of each sample is beyond the scope of this study, variation in the ratio of oleyl chains and fluoride supports a high density of metal fluoride on the QD surface.

In addition to the inorganic fluoride termination, associated amine, ammonium, and phosphonium counterions can provide colloidal stability. Phosphonium, ammonium, and amine ligands can be distinguished using FT-IR spectroscopy by analyzing the v(N–H) region. For instance an authentic sample of *tetrakis*(*n*-hexylamino)phosphonium chloride displays a broad v(N–H) band at 3168 cm^{-1} that is similar to the spectrum of InP QDs purified under anaerobic and aprotic conditions (v(N-H) = 3174 cm^{-1}) (Figures 4A and D). The v(N–H) band of [P(NHR)$_4$]$^+$ is distinct from that of anhydrous oleylammonium chloride which appears as a high frequency shoulder on the oleyl v(C–H) (Figure S21). However, amine ligands coordinated to CdSe nanocrystals have intense v(N–H) bands between 3050 and 3350 cm^{-1}, the same region where [P(NHR)$_4$]$^+$ occurs. All are distinct from v(O–H), which appears in samples exposed to ethanol (~3250–3500 cm^{-1}) (Figure S22). A band at the frequency of v(O–H) has been attributed to v(N–H) in a previous study of InP QDs, but may be the result of contamination by water or ethanol used in the purification.[36] However, a similar amount of oleyl and phosphonium moieties are measured

15

in the ^{1}H and ^{31}P NMR spectra and definitively assign the presence of $[P(NHR)_4]^+$ and rule out surface bound amines/ammoniums.

InP QDs isolated following reaction with $[Oleyl-NH_3]^+[F]^-$ do not contain NMR features associated with phosphonium ions and do contain signals from oleyl chains in both the ^{1}H NMR (Figure S23) and FT-IR spectra. The observed N–H stretching band (ν(N-H) $\approx$ 3134 cm^{-1}) is similar to the spectrum of R-NH$_2$, and distinct from $[R-NH_3]^+[Cl]^-$, $[R-NH_3]^+[BF_4]^-$ (R = oleyl), and $[P(NHR)_4]^+[Cl]^-$ (R = n-hexyl) (Figure 4D). However, the binding of R-NH$_2$ to CdSe QDs dramatically changes the energy and intensity of the ν(N-H), which may explain the broad signal in the 3000–3300 cm^{-1} window of figure 4B, so this assignment is tentative. Moreover, ammonium ions associated with QDs are difficult to distinguish from amines associated with QDs on the basis of FT-IR alone. However, ammonium ions may not be stable ligands for fluoride-terminated InP QDs given that $[Oleyl-NH_3]^+[F]^-$ causes acidolysis of the InP nanocrystal. When isolated metal fluoride terminated QDs are subjected to long term photolysis in the absence of added [Oleyl-NH$_3$]$^+$[F]$^-$ there is no evidence for etching. Thus, we conclude that any associated $[R-NH_3]^+$ ions undergo conversion to amine ligands according to equation 2 and do not remain after the etching process. The FT-IR spectra of fluoride terminated InP QDs in the presence of added oleylamine is shown in Figure 4C. There is little change in the FT-IR lineshape further confirming our assignment. We therefore assign the spectrum in Figure 4B to QDs with surface bound metal fluoride and amine ligands, rather than ammonium fluoride ligands.
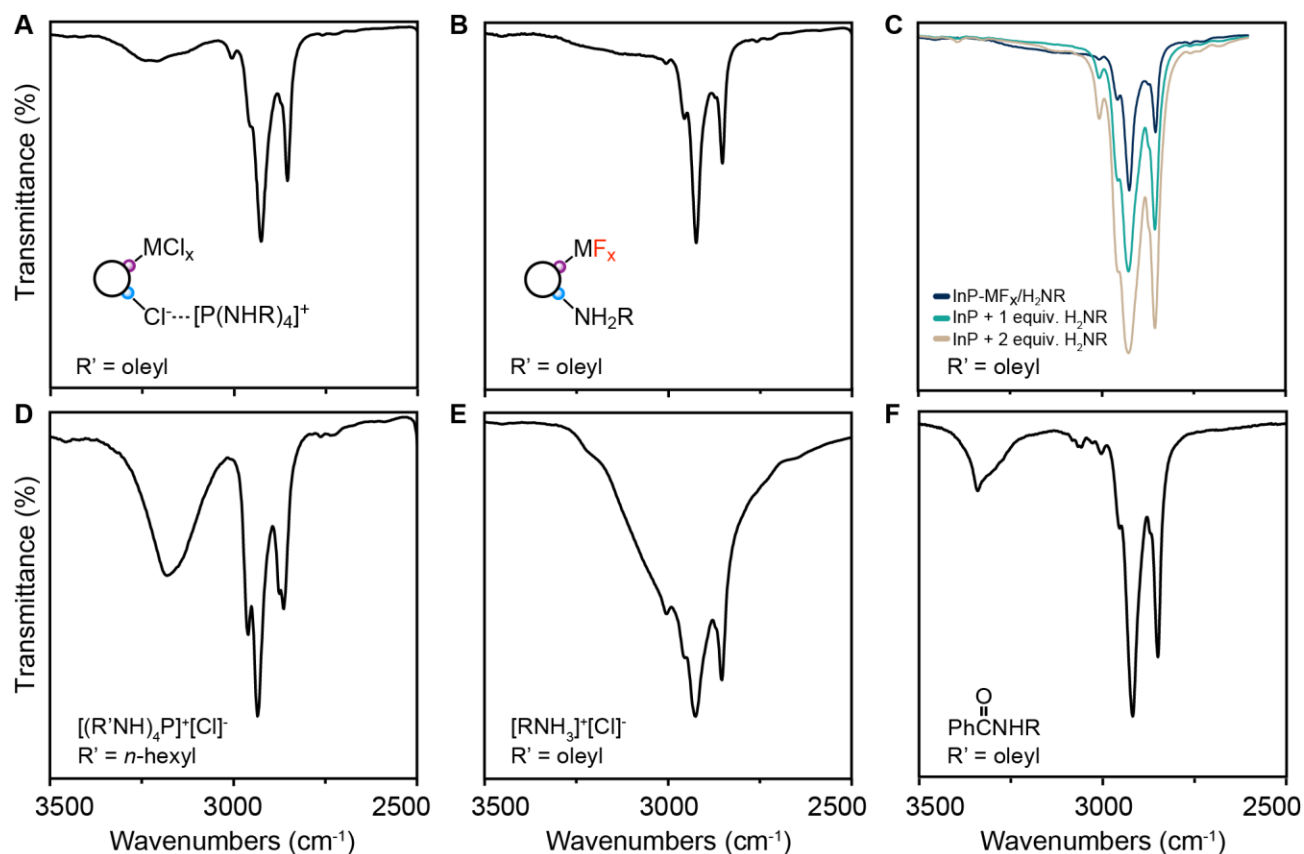
$$(InP)_n/[F]^-[H_3NR]^+ \rightleftharpoons (InP)-H_2NR + 1/3\ InF_3 + 1/3\ PH_3 \qquad (2)$$

16
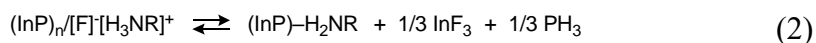
Figure 4. Solution-phase FT-IR spectra in tetrachloroethylene solvent: (**A**) purified **InP-InCl₃/(P(NH-oleyl)₄Cl** QDs 0.4 nm⁻² [P(NHR)₄]⁺, (**B**) **InP-MF_x/R-NH₂**, (**C**) addition of 1 and 2 equivs. H₂N-oleyl /oleyl chain of **InP-MF_x/R-NH₂** QDs, (**D**) *tetrakis*(*n*-hexylamino)phosphonium chloride, (**E**) anhydrous oleylammonium chloride, (**F**) *N*-oleylbenzamide.

Conclusion. The dramatic increase in the PLQY of III-V and II-VI QDs described herein is attributed to the adsorption of MF_x complexes and amine ligands to the QD surface. High aerial density of fluoride ions is achieved suggesting that such metal complexes pack densely on the QD surface. The high packing density helps explain the high PLQYs obtained following fluoride binding. Interestingly, the highest PLQY values obtained for CdS cores were only realized after exposure to air. While photobrightening in the presence of air is well documented a chemical

17

explanation of this brightening is unknown and could shed light on the intricate connection between the coordination chemistry of QD surfaces and their performance in applications.

ASSOCIATED CONTENT

The following files are available free of charge.

Experimental details. ^{1}H, ^{31}P spectra of crude mixtures and products. Discussion on the amine nature, on the sub-stoichiometric amine quantity and on the effect of the surface ligand on the etching behavior. STEM images of described QDs and QWs under several fluorination conditions.

AUTHOR INFORMATION

Corresponding Author

* jso2115@columbia.edu

ORCID

[†] Jonathan S. Owen: 0000-0001-5502-3267

[†,‡] Rodolphe Valleix: 0000-0002-1524-7503

[†] Sungho V. Park: 0000-0002-5949-0548

[†] Bereket L. Zekarias: N/A

[†] William Zhang: N/A

[†,‡] Lilian Guillemeney: N/A

[†] Abraham J. Jordan: 0000-0002-4343-5675

[†] Leslie G. Castro: N/A

[†] Oliver Wang: N/A

Present Addresses

18

† Department of Chemistry, Columbia University, New York, NY 10027, United States.

‡ Univ. Lyon, ENS de Lyon, CNRS, Laboratoire de Chimie, F-69342, Lyon, France.

Author Contributions

The manuscript was written through contributions of all authors. All authors have given approval to the final version of the manuscript.

REFERENCES

(1) Yang, J.; Choi, M. K.; Yang, U. J.; Kim, S. Y.; Kim, Y. S.; Kim, J. H.; Kim, D. H.; Hyeon, T. Toward Full-Color Electroluminescent Quantum Dot Displays. In *Nano Letters*, American Chemical Society: 2021; Vol. 21, pp 26-33.

(2) Jang, E.; Kim, Y.; Won, Y. H.; Jang, H.; Choi, S. M. Environmentally Friendly InP-Based Quantum Dots for Efficient Wide Color Gamut Displays. *ACS Energy Letters* **2020**, *5* (4), 1316-1327. DOI: 10.1021/acsenergylett.9b02851.

(3) Talapin, D. V.; Lee, J.-S.; Kovalenko, M. V.; Shevchenko, E. V. Prospects of Colloidal Nanocrystals for Electronic and Optoelectronic Applications. *Chemical Reviews* **2010**, *110* (1), 389-458. DOI: 10.1021/cr900137k.

19

(4) Moon, H.; Lee, C.; Lee, W.; Kim, J.; Chae, H. Stability of Quantum Dots, Quantum Dot Films, and Quantum Dot Light-Emitting Diodes for Display Applications. *Advanced Materials* **2019**, *31* (34), 1804294. DOI: https://doi.org/10.1002/adma.201804294 (acccessed 2023/10/22).

(5) Anderson, N. C.; Hendricks, M. P.; Choi, J. J.; Owen, J. S. Ligand Exchange and the Stoichiometry of Metal Chalcogenide Nanocrystals: Spectroscopic Observation of Facile Metal-Carboxylate Displacement and Binding. *Journal of the American Chemical Society* **2013**, *135* (49), 18536-18548. DOI: 10.1021/ja4086758.

(6) Busby, E.; Anderson, N. C.; Owen, J. S.; Sfeir, M. Y. Effect of Surface Stoichiometry on Blinking and Hole Trapping Dynamics in CdSe Nanocrystals. *The Journal of Physical Chemistry C* **2015**, *119* (49), 27797-27803. DOI: 10.1021/acs.jpcc.5b08243.

(7) Houtepen, A. J.; Hens, Z.; Owen, J. S.; Infante, I. On the Origin of Surface Traps in Colloidal II–VI Semiconductor Nanocrystals. *Chemistry of Materials* **2017**, *29* (2), 752-761. DOI: 10.1021/acs.chemmater.6b04648.

(8) Kirkwood, N.; Monchen, J. O. V.; Crisp, R. W.; Grimaldi, G.; Bergstein, H. A. C.; du Fossé, I.; van der Stam, W.; Infante, I.; Houtepen, A. J. Finding and Fixing Traps in II–VI and III–V Colloidal Quantum Dots: The Importance of Z-Type Ligand Passivation. *Journal of the American Chemical Society* **2018**, *140* (46), 15712-15723. DOI: 10.1021/jacs.8b07783.

(9) Anderson, N. C.; Chen, P. E.; Buckley, A. K.; De Roo, J.; Owen, J. S. Stereoelectronic Effects on the Binding of Neutral Lewis Bases to CdSe Nanocrystals. *Journal of the American Chemical Society* **2018**, *140* (23), 7199-7205. DOI: 10.1021/jacs.8b02927.

(10) Brown, P. R.; Kim, D.; Lunt, R. R.; Zhao, N.; Bawendi, M. G.; Grossman, J. C.; Bulović, V. Energy Level Modification in Lead Sulfide Quantum Dot Thin Films through Ligand Exchange. *ACS Nano* **2014**, *8* (6), 5863-5872. DOI: 10.1021/nn500897c.

(11) Schmidt, R.; Oh, J. H.; Sun, Y.-S.; Deppisch, M.; Krause, A.-M.; Radacki, K.; Braunschweig, H.; Könemann, M.; Erk, P.; Bao, Z.; et al. High-Performance Air-Stable n-Channel Organic Thin Film Transistors Based on Halogenated Perylene Bisimide Semiconductors. *Journal of the American Chemical Society* **2009**, *131* (17), 6215-6228. DOI: 10.1021/ja901077a.

(12) Ning, Z.; Voznyy, O.; Pan, J.; Hoogland, S.; Adinolfi, V.; Xu, J.; Li, M.; Kirmani, A. R.; Sun, J.-P.; Minor, J.; et al. Air-stable n-type colloidal quantum dot solids. *Nature Materials* **2014**, *13* (8), 822-828. DOI: 10.1038/nmat4007.

(13) Ghosh, S.; Manna, L. The Many "Facets" of Halide Ions in the Chemistry of Colloidal Inorganic Nanocrystals. *Chemical Reviews* **2018**, *118* (16), 7804-7864. DOI: 10.1021/acs.chemrev.8b00158.

(14) Rreza, I.; Yang, H.; Hamachi, L.; Campos, M.; Hull, T.; Treadway, J.; Kurtin, J.; Chan, E. M.; Owen, J. S. Performance of Spherical Quantum Well Down Converters in Solid State

20

Lighting. *ACS Applied Materials & Interfaces* **2021**, *13* (10), 12191-12197. DOI: 10.1021/acsami.0c15161.

(15) Orfield, N. J.; Majumder, S.; Hu, Z.; Koh, F. Y.-C.; Htoon, H.; Hollingsworth, J. A. Kinetics and Thermodynamics of Killing a Quantum Dot. *ACS Applied Materials & Interfaces* **2020**, *12* (27), 30695-30701. DOI: 10.1021/acsami.0c05980.

(16) Adam, S.; Talapin, D. V.; Borchert, H.; Lobo, A.; McGinley, C.; De Castro, A. R. B.; Haase, M.; Weller, H.; Möller, T. The effect of nanocrystal surface structure on the luminescence properties: Photoemission study of HF-etched InP nanocrystals. *Journal of Chemical Physics* **2005**, *123* (8). DOI: 10.1063/1.2004901.

(17) Won, Y. H.; Cho, O.; Kim, T.; Chung, D. Y.; Kim, T.; Chung, H.; Jang, H.; Lee, J.; Kim, D.; Jang, E. Highly efficient and stable InP/ZnSe/ZnS quantum dot light-emitting diodes. *Nature* **2019**, *575* (7784), 634-638. DOI: 10.1038/s41586-019-1771-5.

(18) Xie, L.; Harris, D. K.; Bawendi, M. G.; Jensen, K. F. Effect of Trace Water on the Growth of Indium Phosphide Quantum Dots. *Chemistry of Materials* **2015**, *27* (14), 5058-5063. DOI: 10.1021/acs.chemmater.5b01626.

(19) Virieux, H.; Le Troedec, M.; Cros-Gagneux, A.; Ojo, W.-S.; Delpech, F.; Nayral, C.; Martinez, H.; Chaudret, B. InP/ZnS Nanocrystals: Coupling NMR and XPS for Fine Surface and Interface Description. *Journal of the American Chemical Society* **2012**, *134* (48), 19701-19708. DOI: 10.1021/ja307124m.

(20) Click, S. M.; Rosenthal, S. J. Synthesis, Surface Chemistry, and Fluorescent Properties of InP Quantum Dots. *Chemistry of Materials* **2023**, *35* (3), 822-836. DOI: 10.1021/acs.chemmater.2c03074.

(21) Siramdas, R.; McLaurin, E. J. InP Nanocrystals with Color-Tunable Luminescence by Microwave-Assisted Ionic-Liquid Etching. *Chemistry of Materials* **2017**, *29* (5), 2101-2109. DOI: 10.1021/acs.chemmater.6b04457.

(22) Lovingood, D. D.; Strouse, G. F. Microwave induced In-Situ active ion etching of growing inP nanocrystals. *Nano Letters* **2008**, *8* (10), 3394-3397. DOI: 10.1021/nl802075j.

(23) Chandrasiri, H. B.; Kim, E. B.; Snee, P. T. Sterically encumbered tris(trialkylsilyl) phosphine precursors for quantum dot synthesis. *Inorganic Chemistry* **2020**, *59* (21), 15928-15935. DOI: 10.1021/acs.inorgchem.0c02440.

(24) Li, H.; Zhang, W.; Bian, Y.; Ahn, T. K.; Shen, H.; Ji, B. ZnF2-Assisted Synthesis of Highly Luminescent InP/ZnSe/ZnS Quantum Dots for Efficient and Stable Electroluminescence. *Nano Letters* **2022**, *22* (10), 4067-4073. DOI: 10.1021/acs.nanolett.2c00763.

(25) Van Avermaet, H.; Schiettecatte, P.; Hinz, S.; Giordano, L.; Ferrari, F.; Nayral, C.; Delpech, F.; Maultzsch, J.; Lange, H.; Hens, Z. Full-Spectrum InP-Based Quantum Dots with Near-Unity

21

Photoluminescence Quantum Efficiency. *ACS Nano* **2022**. DOI: 10.1021/acsnano.2c03138 From NLM Publisher.

(26) Reinout F. Ubbink, G. A., Hodayfa Iziyi, Indy du Fossé, Ruud Verkleij, Swapna Ganapathy, Ernst R. H. van Eck, and Arjan J. Houtepen*. A Water-Free In Situ HF Treatment for Ultrabright InP Quantum Dots. *Chem. Mater* **2022**, *34*, 10093−10103. DOI: doi.org/10.1021/acs.chemmater.2c02800.

(27) Wei, L.; Ye, J.; Zhou, X.; Guo, T.; Ren, C.; Yan, Q.; Zhang, Y.; Wu, C. Improved luminescent InP/ZnS quantum dots by ZnF2 assisted one-pot aminophosphine synthesis strategy. *Optical Materials* **2022**, *134*, 113209. DOI: https://doi.org/10.1016/j.optmat.2022.113209.

(28) Hamachi, L. S.; Yang, H.; Jen-La Plante, I.; Saenz, N.; Qian, K.; Campos, M. P.; Cleveland, G. T.; Rreza, I.; Oza, A.; Walravens, W.; et al. Precursor reaction kinetics control compositional grading and size of CdSe1-: XSx nanocrystal heterostructures. *Chemical Science* **2019**, *10* (26), 6539-6552. DOI: 10.1039/c9sc00989b.

(29) Hamachi, L. S.; Jen-La Plante, I.; Coryell, A. C.; De Roo, J.; Owen, J. S. Kinetic Control over CdS Nanocrystal Nucleation Using a Library of Thiocarbonates, Thiocarbamates, and Thioureas. *Chemistry of Materials* **2017**, *29* (20), 8711-8719. DOI: 10.1021/acs.chemmater.7b02861.

(30) Nefedov V.I., B. Y. A., Kokunov Y.V. *Zh. Neorg. Khimii* **1974**, *19*, 1166.

(31) Cros-Gagneux, A.; Delpech, F.; Nayral, C.; Cornejo, A.; Coppel, Y.; Chaudret, B. Surface Chemistry of InP Quantum Dots: A Comprehensive Study. *Journal of the American Chemical Society* **2010**, *132* (51), 18147-18157. DOI: 10.1021/ja104673y.

(32) Clarke, M. T.; Viscomi, F. N.; Chamberlain, T. W.; Hondow, N.; Adawi, A. M.; Sturge, J.; Erwin, S. C.; Bouillard, J.-S. G.; Tamang, S.; Stasiuk, G. J. Synthesis of super bright indium phosphide colloidal quantum dots through thermal diffusion. *Communications Chemistry* **2019**, *2* (1), 36. DOI: 10.1038/s42004-019-0138-z.

(33) Tarantini, A.; Wegner, K. D.; Dussert, F.; Sarret, G.; Beal, D.; Mattera, L.; Lincheneau, C.; Proux, O.; Truffier-Boutry, D.; Moriscot, C.; et al. Physicochemical alterations and toxicity of InP alloyed quantum dots aged in environmental conditions: A safer by design evaluation. *NanoImpact* **2019**, *14*, 100168. DOI: https://doi.org/10.1016/j.impact.2019.100168.

(34) Tessier, M. D.; Baquero, E. A.; Dupont, D.; Grigel, V.; Bladt, E.; Bals, S.; Coppel, Y.; Hens, Z.; Nayral, C.; Delpech, F. Interfacial Oxidation and Photoluminescence of InP-Based Core/Shell Quantum Dots. *Chemistry of Materials* **2018**, *30* (19), 6877-6883. DOI: 10.1021/acs.chemmater.8b03117.

(35) Tessier, M. D.; Dupont, D.; De Nolf, K.; De Roo, J.; Hens, Z. Economic and Size-Tunable Synthesis of InP/ZnE (E = S, Se) Colloidal Quantum Dots. *Chemistry of Materials* **2015**, *27* (13), 4893-4898. DOI: 10.1021/acs.chemmater.5b02138.

22

(36) Dümbgen, K. C.; Infante, I.; Hens, Z. Localizing Oleylamine Ligands on Amine–Halide Copassivated Indium Phosphide Nanocrystals. *Chemistry of Materials* **2023**, *35* (11), 4393-4403. DOI: 10.1021/acs.chemmater.3c00565.

(37) Dümbgen, K. C.; Leemans, J.; De Roo, V.; Minjauw, M.; Detavernier, C.; Hens, Z. Surface Chemistry of InP Quantum Dots, Amine–Halide Co-Passivation, and Binding of Z-Type Ligands. *Chemistry of Materials* **2023**, *35* (3), 1037-1046. DOI: 10.1021/acs.chemmater.2c02960.

(38) Kieser, J. M.; Gilliard, R. J.; Rheingold, A. L.; Grützmacher, H.; Protasiewicz, J. D. Insertion of sodium phosphaethynolate, Na[OCP], into a zirconium-benzyne complex. *Chemical Communications* **2017**, *53* (37), 5110-5112. DOI: 10.1039/c7cc01482a.

(39) Rothfelder, R.; Streitferdt, V.; Lennert, U.; Cammarata, J.; Scott, D. J.; Zeitler, K.; Gschwind, R. M.; Wolf, R. Photocatalytic Arylation of P4 and PH3: Reaction Development Through Mechanistic Insight. *Angewandte Chemie - International Edition* **2021**, *60* (46), 24650-24658. DOI: 10.1002/anie.202110619.

(40) Scott, D. J.; Cammarata, J.; Schimpf, M.; Wolf, R. Synthesis of monophosphines directly from white phosphorus. *Nature Chemistry* **2021**, *13* (5), 458-464. DOI: 10.1038/s41557-021-00657-7.

(41) Liotta L. Charles, M. L. M. O. B. A. B. The synthesis and reactions of potassium benzoylphosphide, benzoylphosphine, and benzoylmethylphosphine. *tetrahedron letters* **1984**, *25* (12), 1249-1252.

(42) Piotr Garbacz, a. W. M. a. M. J. s. The NMR spin–spin coupling constant 1J(31P,1H) in an isolated PH3 molecule. *Phys. Chem. Chem. Phys.* **2014**, *16*, 21559.

(43) Kühl, O. *Phosphorus-31 NMR Spectroscopy*; 2008.

(44) Dempsey, S. H.; Kass, S. R. Liberating the Anion: Evaluating Weakly Coordinating Cations. *The Journal of Organic Chemistry* **2022**, *87* (22), 15466-15482. DOI: 10.1021/acs.joc.2c02001.

(45) Yadav, R.; Kwon, Y.; Rivaux, C.; Saint-Pierre, C.; Ling, W. L.; Reiss, P. Narrow Near-Infrared Emission from InP QDs Synthesized with Indium(I) Halides and Aminophosphine. *Journal of the American Chemical Society* **2023**, *145* (10), 5970-5981. DOI: 10.1021/jacs.2c13834.

(46) Ubbink, R. F.; Almeida, G.; Iziyi, H.; du Fossé, I.; Verkleij, R.; Ganapathy, S.; van Eck, E. R. H.; Houtepen, A. J. A Water-Free In Situ HF Treatment for Ultrabright InP Quantum Dots. *Chemistry of Materials* **2022**, *34* (22), 10093-10103. DOI: 10.1021/acs.chemmater.2c02800.

(47) Talapin, D. V.; Gaponik, N.; Borchert, H.; Rogach, A. L.; Haase, M.; Weller, H. Etching of Colloidal InP Nanocrystals with Fluorides: Photochemical Nature of the Process Resulting in

23

High Photoluminescence Efficiency. *The Journal of Physical Chemistry B* **2002**, *106* (49), 12659-12663. DOI: 10.1021/jp026380n.

(48) Adam, S.; Talapin, D. V.; Borchert, H.; Lobo, A.; McGinley, C.; de Castro, A. R. B.; Haase, M.; Weller, H.; Möller, T. The effect of nanocrystal surface structure on the luminescence properties: Photoemission study of HF-etched InP nanocrystals. *The Journal of Chemical Physics* **2005**, *123* (8), 084706. DOI: 10.1063/1.2004901 (acccessed 11/4/2023).

(49) Miller, J. M. Fluorine-19 magic-angle spinning NMR. *Progress in Nuclear Magnetic Resonance Spectroscopy* **1996**, *28* (3), 255-281. DOI: https://doi.org/10.1016/0079-6565(95)01024-6.

(50) Luo, Y.-R. *Comprehensive Handbook of Chemical Bond Energies*; CRC Press, 2007. DOI: https://doi.org/10.1201/9781420007282.

TOC GRAPHIC